https://doi.org/10.5194/egusphere-2026-3457
Preprint. Discussion started: 18 August 2026

Rainfall monitoring based on spectral analysis of sound recordings in different geographical locations

Rodrigo S. Xavier[1], Ayan S. Fleischmann[2], Marielle Gosset[3], Tarcísio F. Maciel[1], Modeste Kacou[4], Tamna G. Silva[2], Kouassi T. Tewa[4]

[1]Universidade Federal do Ceará, Fortaleza, Ceará, Brazil
[2]Instituto de Desenvolvimento Sustentável Mamirauá, Tefé, Amazonas, Brazil
[3] IRD, CNRS, UT3, CNES, Paris, France
[4]Université Félix Houphouët-Boigny, Abidjan, Côte d'Ivoire

Correspondence to: Rodrigo S. Xavier (rodrigoxavierlt@gmail.com)

Abstract. Recent interest in geophony-based approaches for rainfall monitoring has highlighted its potential as a low-cost complement to traditional methods. Yet, most existing techniques rely on model training and lack cross-site validation. In this study, we introduce and evaluate a simple acoustic metric for rainfall characterization based on deviations in power spectral density from a local baseline under dry-weather conditions. The method was applied to eight datasets containing audio recordings from tropical and temperate forests, as well as urban and semi-urban environments, and validated using rain gauge measurements. Results show consistently high correlations (≈ 0.7) between the proposed metric and rainfall rate for the tropical (Amazonian and West African) datasets when low-frequency bands are chosen (0.2-0.5 kHz), as opposed to the open-air dataset, which did not present significant correlation values. Additionally, for the temperate forest dataset (France), higher correlations are obtained on the higher part of the spectra (3.2-3.5 kHz), likely due to wind and technophonic-related interferences (jet engine background noise) at lower frequencies. Although common frequency bands are identified across multiple sites, the amplitude of the proposed metric varies substantially between regions, indicating that a universal physical relationship for direct rainfall rate estimation may be difficult to achieve. These results highlight both the potential and the limitations of a simple, training-free acoustic metric for rainfall monitoring across diverse environments.

1 Introduction

Accurate and continuous meteorological data is essential for a wide range of applications, including improving weather forecasts and timely severe weather warnings, as well as enabling effective decision-making in water resource management and agricultural planning. However, due to its high spatio-temporal variability, collecting reliable surface precipitation data remains a significant challenge, leading to difficulties in its accurate prediction. Although the global observational network has expanded coverage in the last five years (WMO, 2025), the lack of data still introduces uncertainties about future increases in extreme precipitation events linked to climate change, particularly in developing

https://doi.org/10.5194/egusphere-2026-3457
Preprint. Discussion started: 18 August 2026

countries (Calvin et al., 2023). Moreover, monitoring infrastructure remains highly concentrated in developed nations (WMO, 2023), further adding to the global data inequality and disproportionately affecting vulnerable regions that are more susceptible to the impacts of climate change (Adom, 2024; Pinho et al., 2025).

Several different instruments are available for measuring rainfall (Rácz & Waltner, 2023), the most widely employed is the rain gauge, which directly collects and measures precipitation. Other indirect methods estimate rainfall rates based on physical properties; these include ground-based approaches, which include local approaches, such as disdrometers, as well as remote sensing methods that utilize weather radars and satellites. Each technique comes with its own set of limitations. Rain gauges may suffer from wind-induced measurement errors, weather radars are expensive to operate and maintain, and satellites often lack the temporal resolution needed to capture intra-hour rainfall variability.

In recent years, innovative and opportunistic rainfall measurement techniques have emerged to complement traditional observations, such as using audio-based methods, which utilize recordings and machine learning or modern deep-learning architectures to obtain rainfall intensity, with applications in urban (Alkhatib et al., 2024; Guo et al., 2019; Hwang et al., 2024; M. Wang et al., 2024) and forest environments (Bedoya et al., 2017; Metcalf et al., 2020; Xavier et al., 2024). Other studies employ direct acoustic sensing to monitor rain inclination of wind-driven precipitation in real time (Dunkerley, 2026) and other environmental variables such as wind speed (Wang et al., 2026). These studies highlight the ecoacoustics of a given soundscape as a low-cost method for obtaining meteorological data.

Despite promising results, significant limitations remain. Most studies focus primarily on rainfall classification (Aquino et al., 2022; Avanzato & Beritelli, 2020; Chen et al., 2022), leaving the more useful and difficult task of quantitative rainfall estimation underexplored. Additionally, a significant share of the existing literature relies on datasets from simulated rainfall (Avanzato et al., 2019; Capin & Dimaunahan, 2023; X. Wang et al., 2023), which may not fully represent the acoustic complexity of real-world events. Furthermore, only a small number of studies have performed cross-site validation (Alkhatib et al., 2023, 2024; Hwang et al., 2024; Wang et al., 2024; Xavier et al., 2024), making it difficult to evaluate the generalizability of models across different environments.

The present study investigated whether a simple, training-free acoustic metric can be generalized across a diverse range of environmental conditions. Instead of relying on model training, the proposed approach is based on normalizing the acoustic spectra against a locally derived baseline of dry-weather conditions, requiring only a brief period of previously known dry-weather for calibration. The method is evaluated across eight datasets, encompassing tropical and temperate forest environments, as well as semi-urban settings, allowing for a systematic evaluation of its performance and limitations in relation to environmental factors such as vegetation structure and wind. This paper is organized as follows: Section 2 describes the methodology, including the study regions, recording setups, rain gauge instrumentation, and the formulation of the proposed acoustic metric. Section 3 presents the results, including the characterization of the data collection period, optimization of the frequency window, cross-site generalization experiments, and a discussion of the main identified limitations. Section 4 summarizes the main findings and outlines directions for future work.

https://doi.org/10.5194/egusphere-2026-3457
Preprint. Discussion started: 18 August 2026

2 Methodology

2.1 Study Areas

The present study is based on eight datasets (Table 1), six of them collected in tropical environments and two in temperate settings. Four of these were collected in the central Amazon region of Brazil, characterized by an Af Köppen climate type (tropical rainforest without a dry season, Alvares et al., 2013. The first of the four Amazonian datasets was collected in a secondary tropical rainforest (Fig. 1a) located within the premises of the Mamirauá Institute for Sustainable Development (IDSM), in the city of Tefé, State of Amazonas. Tefé is situated approximately 550 km west of the state capital, Manaus, and experiences a mean annual rainfall of about 2,500 mm, with the wettest period occurring between December and April, driven by local convection, Intertropical Convergence Zone (ITCZ), squall lines, and Mesoscale Convective Complexes (Reboita et al., 2010). The second, third, and fourth datasets were collected within the Mamirauá Sustainable Development Reserve (MDSR), approximately 40 km north of the IDSM site. MDSR is mainly characterized by three distinct vegetation types (Ferreira-Ferreira et al., 2015). Chavascal (CH) consists primarily of dense, species-poor shrubs and trees (Fig. 1b). The Low Várzea (LV) habitat supports fewer and smaller plant species (Fig. 1c) compared to the High Várzea (HV), which is characterized by a more complex and vertically structured canopy, with a higher diversity of species (Fig. 1d).

Completing the Brazilian sites, the fifth dataset was collected on the campus of the Ceará State University (UECE), located in the city of Fortaleza (Fig. 1e), on the northeastern coast of Brazil. This presents an As Köppen climate (tropical climate with a dry summer). It has a mean annual precipitation of approximately 1,500 mm, with rainfall primarily driven by the seasonal migration of the ITCZ during the first half of the year, as well as sea-breeze-induced convective activity (Reboita et al., 2010).

The sixth dataset was collected in Abidjan (ABJ), in southern Ivory Coast (West Africa). The region presents a tropical climate with a dry winter (Beck et al., 2018), and is strongly influenced by the seasonal displacement of the ITCZ and coastal sea-breeze processes. Rainfall in Abidjan follows a bimodal annual cycle, with a major rainy season between April and July (with a maximum of 600 mm per month), and a secondary peak of approximately 200 mm in October (Kouadio et al., 2011).

The seventh and eighth datasets were collected in the city of Toulouse (TLS), located in the Occitanie region of Southern France. The region is classified as Cfa according to the Köppen climate classification, with a humid subtropical climate, without a dry season, and with a hot summer (Beck et al., 2018). This mid-latitude site is characterized by relatively low total annual precipitation (below 800 mm), influenced by both Atlantic and Mediterranean weather systems. Rainfall occurs more frequently during winter months, typically associated with stratiform oceanic precipitation. In contrast, summer months (June to September) exhibit fewer rainy days but are characterized by more intense events (Joly et al., 2010). The main distinction between these datasets is related to local vegetation structure: one deployment (TLS-1) is located within a

https://doi.org/10.5194/egusphere-2026-3457
Preprint. Discussion started: 18 August 2026

patch of vegetation characterized by a higher and more open canopy (Fig. 1g), the second (TLS-2) was installed a few meters away in an area with denser vegetation and a lower canopy (Fig. 1h).

2.2 Experimental setups

2.2.1 Acoustic data

Table 1 presents a summary of the recording parameters and data collection period. Audio information was collected using seven autonomous recorders of two different models. The first is the Song Meter Micro (SMM), produced by Wildlife Acoustics, with built-in omnidirectional microphones (sensitivity: +2 dB FS ±4 dB; Signal-to-Noise Ratio: 73 dB). The second is the AudioMoth recorder, which is a mono recorder that can record using up to 16 bits/sample, a maximum sampling frequency of 384 kHz, and is equipped with a built-in Micro Electrical-Mechanical System microphone. Original sampling rates ranged from 16 to 48 kHz (Table 1); all of the analyses of the recordings were performed after an audio downsampling to 16 kHz to ensure methodological consistency, and the length of recordings varied from 1 minute every five minutes (IDSM, CH, LV, HV, and TLS) to 30 seconds every 2.5 minutes (ABJ). Audio recordings were collected intermittently at fixed intervals, which vary slightly across sites: most datasets use a 5-minute interval and 1-minute recordings. In contrast, the Abidjan (ABJ) dataset was collected with timesteps of 2.5 minutes and 30-second recordings.

Figure 1 illustrates the locations and experimental setups for the study areas. Recorders were installed in proximity to rain gauges, which provided ground-truth rainfall measurements. The acoustic environment varies across datasets. The IDSM dataset contains a higher proportion of anthropophonic and technophonic sounds compared to the more isolated MDSR (CH, LV, and HV) sites, where technophonic noise is primarily associated with boat engines. The UECE, ABJ, and TLS datasets include sounds from road traffic and human activity, with the TLS datasets showing the highest contribution from machinery and engine-related background noise.

https://doi.org/10.5194/egusphere-2026-3457
Preprint. Discussion started: 18 August 2026

116

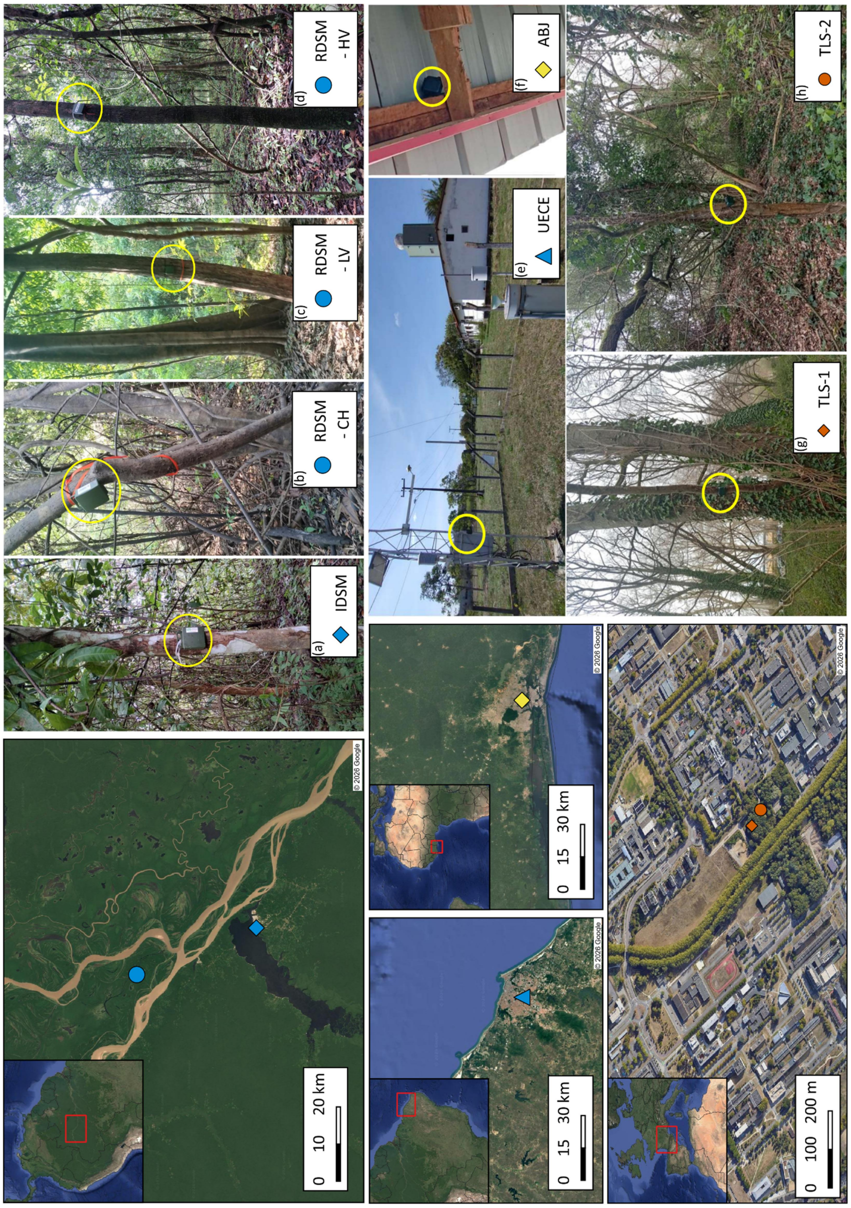

Figure 1: Set of maps and photos depicting all eight experimental setups.

https://doi.org/10.5194/egusphere-2026-3457
Preprint. Discussion started: 18 August 2026

2.2.2 Rain gauge data

For every site, rainfall data were collected with a Tipping Bucket Rain Gauge (TBRG), with site-specific instrumentation. At the Amazonian sites, rainfall was measured using the pluvDB gauge (DualBase, Palhoça, SC, Brazil), with a resolution of 0.2 mm every 5 minutes. At the UECE site, a TB4MM gauge (Campbell Scientific Brazil, São Paulo, SP, Brazil) was used, with a resolution of 0.2 mm every 5 minutes. At the ABJ site, a Précis Mécanique® model 3039 (Précis Mécanque, Bezons, IDF, France) was used, with a resolution of 0.5 mm and a 2.5-minute interval. At the TLS sites, rainfall was recorded using the TBRG integrated into the Wireless Vantage Pro2™ weather station (Davis Instruments, Hayward, CA, USA), with a resolution of 0.2 mm every 5 minutes.

Data collection includes the total amount of data collected and the number of rainfall events. A rainfall event was defined as a period with measurable precipitation lasting at least 6 consecutive rain gauge timesteps. Events were separated by a minimum inter-event time (MIT) of 1 hour, defined as the minimum duration with no recorded rainfall required to separate two consecutive events. While rainfall event definitions and results are known to be sensitive to the choice of inter-event time, local precipitation regimes, and the specific research objective (Dunkerley, 2008), the goal of this study is not to provide an in-depth analysis of rainfall event distributions or to determine an optimal MIT for each site. Instead, a single MIT value was adopted to ensure methodological consistency across all datasets, which span both tropical (Amazon region, northeastern Brazil, Abidjan) and mid-latitude (Toulouse) environments, for which no single inter-event time can be considered universally optimal. Overall, the 1-hour MIT provides a reasonable compromise between separating independent rainfall episodes and avoiding excessive fragmentation of prolonged events.

https://doi.org/10.5194/egusphere-2026-3457
Preprint. Discussion started: 18 August 2026

Table 1. Summary of recording parameters, environments, and data collected.

Dataset	Country	Climate	Environment	Coordinates	Recorder	Sampling rate (kHz)	Period	Total hours	Wet hours	Total rainfall (mm)	Number of rainfall events
IDSM	Brazil	Af	Secondary tropical forest	3.35349° S 64.73285° W	SMM Wildlife	48	2023-02-14 to 2024-10-25	1201	33.1	1168	55
CH			Pristine tropical forest	3.065828° S 64.847753° W	SMM Wildlife	24	2024-01-12 to 2024-05-26	95	3.6	210	7
LV			Pristine tropical forest	3.065829° S 64.847346° W	SMM Wildlife	24	2023-12-11 to 2024-05-27	202	5.8	324	13
HV			Pristine tropical forest	3.06199° S 64.84573° W	SMM Wildlife	24	2023-12-11 to 2024-04-12	227	7.4	527	8
UECE		As	Open-air, semi-urban	3.795124° S 38.5557381° W	SMM Wildlife	24	2025-02-27 to 2025-08-02	507	18.4	981	29
ABJ	Ivory Coast	Aw	Urban, roof-covered	5.3441258° N 3.9895281° W	AudioMoth	32	2024-04-22 to 2024-10-07	503	3.9	435	8
TLS-1	France	Cfa	Urban patch of temperate forest	43.561204° N 1.475657° E	AudioMoth	16	2025-11-05 to 2026-05-11	236	13.8	270	19
TLS-2			Urban patch of temperate forest	43.561016° N 1.476318° E	AudioMoth	16	2025-10-22 to 2026-05-11	296	14.7	282	20

https://doi.org/10.5194/egusphere-2026-3457
Preprint. Discussion started: 18 August 2026

2.3 Algorithm

Power Spectrum Density (PSD) has been widely used as a feature in both classical machine learning and deep learning models to detect and estimate rainfall using sound recorders (Bedoya et al., 2017; Brown et al., 2019; Guo et al., 2019; Metcalf et al., 2020; Xavier et al., 2024). In this study, we adapt the methodology proposed by Chwala et al. (2012) and Schleiss & Berne (2010), in which the authors applied a PSD baseline to received signal levels from commercial microwave links to determine wet and dry periods. PSD values were obtained from each recording by employing Welch's method, available in the Signal module from the Scipy library (Virtanen et al., 2020), with a number of samples per segment parameter (nperseg) set to 1024.

Let $S(f,t)$ be the PSD of the audio recording at a time t for a given frequency f, h the hour of the day ($h \in \{0,1,\ldots,23\}$), and D_h the set of all dry-period audio recordings during the hour h. By calculating hourly baselines, we account for dry fluctuations originating from biophonic sources (e.g., insects, such as cicadas, are more active at night). The hourly mean dry PSD, $\bar{S}_{dry}(f,h)$, is obtained as the average PSD across all dry recordings for that specific hour:

$$\bar{S}_{dry}(f,h) = \frac{1}{|D_h|}\sum_{t\in D_h} S(f,t), \quad (1)$$

where $|D_h|$ is the total number of dry-period recordings in the set D_h. As proposed by Chwala et al. (2012), the normalized PSD for each point in time t, $S_{norm}(f,t)$, is given by:

$$S_{norm}(f,t) = \frac{S(f,t)}{\bar{S}_{dry}(f,h)}, \quad (2)$$

In this study, the dry-weather baseline was constructed by randomly selecting 100 samples from each hour of the day. This number was empirically chosen to provide a sufficiently representative baseline while avoiding the need for a long previously known dry period. Other factors could be taken into consideration when building the dry baseline, such as local seasonal variability. In this context, an important consideration is how much does the environment change throughout the year. For the Amazonian datasets there is no significant change in the canopy or foliage cover throughout the year, however, a factor that could influence the dry baseline is the flooding season inside the RDSM, but the limited deployment period renders this effect negligible. In contrast, the TLS datasets were collected in a temperate setting, therefore their monitoring sites may experience significant changes in canopy density, and it would be interesting to verify how these variations affect the dry baseline for longer deployment periods.

To illustrate the proposed methodology in practice, Fig. 2 shows results for the average daily cycle of the dry-weather baseline for the IDSM dataset, following the use of Eq. (1). It displays clear diurnal variations in the PSD (Fig. 2a). Also, a pronounced nocturnal signature is observed between 17:00 and 09:00, with increased energy in the 3-8 kHz

https://doi.org/10.5194/egusphere-2026-3457
Preprint. Discussion started: 18 August 2026

frequency range. This is consistent with increased bioacoustic activity during nighttime, such as cicadas (Fig. A1). The application of Eq. (2) to four randomly selected samples, two associated with light and heavy rainfall and two dry recordings from the same hour (Fig. 2b and 2c), highlights systematic differences between wet and dry conditions. The contrast between wet and dry audios is evident, and these particular examples indicate that the spectral differences remain relatively uniform across most of the analyzed frequency range.

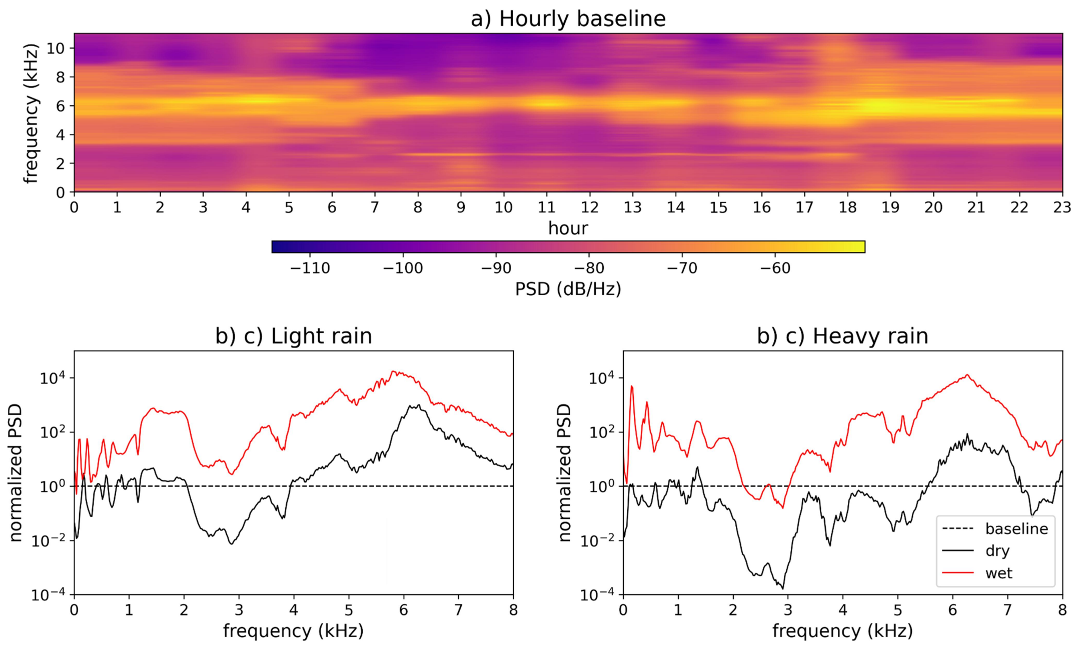

Figure 2: Average daily cycle of the PSD dry-weather baseline (a) based on Eq. (1), and normalized PSD (Eq. 2) of two randomly selected samples of light (b) and heavy (c) rain for the IDSM dataset.

Chwala et al. (2012) used a differential metric to determine whether a period is dry or wet, based on strong deviations in normalized wet spectra at both high and low frequencies. In contrast, we simply obtain the average of the normalized PSD within a frequency range ($\hat{S}$):

$$\hat{S} = \frac{1}{N_{range}} \sum_{f \in F_{range}} S_{norm}(f,t) \qquad (3)$$

https://doi.org/10.5194/egusphere-2026-3457
Preprint. Discussion started: 18 August 2026

where F_{range} is the set of frequency bins between a certain f_{min} and f_{max}, and N_{range} the total number of frequency bins in Frange. We classify the time t as wet or dry by comparing the value $\hat{S}(t)$ to an empirically derived threshold σ, based on the p^{th} percentile of $\hat{S}(t)$ values observed during dry periods:

$$t = \begin{cases} wet\ if\ \hat{S}(t) > \sigma \\ dry\ if\ \hat{S}(t) \leq \sigma \end{cases} \tag{4}$$

A similar approach was used by Schleiss & Berne (2010) in the context of microwave links for rainfall detection, where the authors defined a wet/dry threshold based on the 99th quantile of the signal's local standard deviation during dry periods.

2.4 Example of algorithm implementation

Figure 3 illustrates the empirical metric applied to a rainfall event from the IDSM dataset, which occurred between February 16, 2023, 18:30 and February 17, 2023, 07:50. The metric was computed using a manually selected threshold ($\sigma = 0.95$) and a frequency band from 0 to 4 kHz. An optimization of these parameters is presented in Section 3.3. The event corresponds to a convective rainfall episode characterized by two precipitation peaks of 0.8 mm per 5 minutes (equivalent to 9.6 mm h^{-1}), which occurred on February 16, 20:25, and 17 February, 02:55. Despite these empirically chosen values, the proposed metric exhibits a strong correspondence with the ground-truth measurements and accurately captures the beginning and end of the rainfall event.

https://doi.org/10.5194/egusphere-2026-3457
Preprint. Discussion started: 18 August 2026

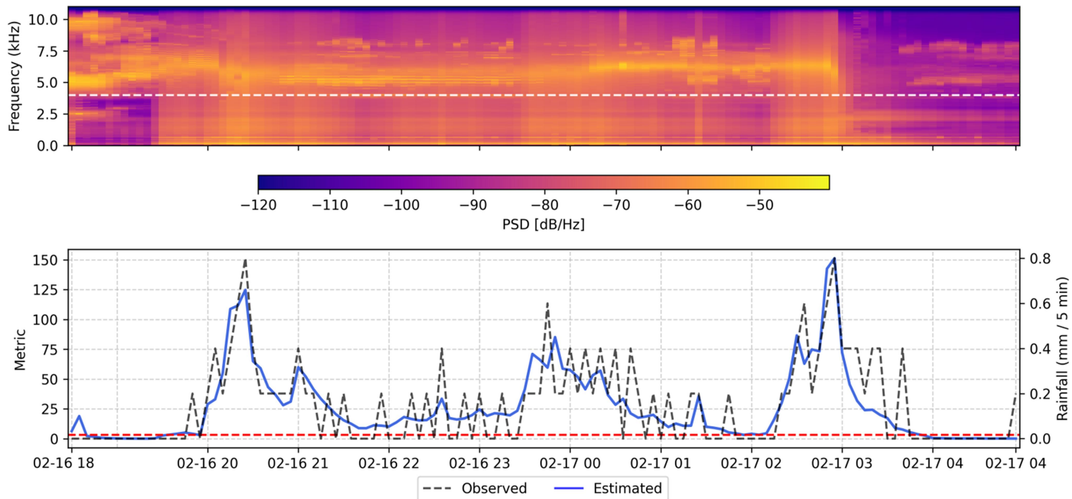

Figure 3: Example of the proposed rainfall metric applied to a rainfall event in the central Amazon region (IDSM dataset). The top plot depicts the time series of the PSD extracted from audio recordings, and the dashed white line represents the frequency cut at 4 kHz. The bottom plot displays the time series of rainfall intensity (dashed black line), along with the sound-based rainfall metric (blue line) and the σ threshold (dashed red line), above which an audio is classified as wet.

2.5 Sensitivity tests and performance metrics

To validate the capability of our empirical metric to identify wet and dry periods, we employed the same concept as the one proposed in Chwala et al. (2012), where the authors defined the error rate mean as a weighted mean between the false positives and false negatives:

$$\varepsilon_{\omega mean} = \omega\varepsilon_{wet} + (1-\omega)\varepsilon_{dry}, \tag{4}$$

where

$$\varepsilon_{wet} = \frac{FN}{TP+FN} \tag{5}$$

and

https://doi.org/10.5194/egusphere-2026-3457
Preprint. Discussion started: 18 August 2026

$$\varepsilon_{dry} = \frac{FP}{TN+F} \quad (6)$$

with FN and TN denoting the false and true negatives, respectively, and FP and TP the false and true positives, respectively. As proposed by Chwala et al. (2012), the weighting factor ω is set to 0.6, prioritizing the error of wet detection. While the error rate assesses the binary accuracy of the wet/dry classification, we further evaluated the ability of the empirical metric to track rainfall intensity by calculating the Pearson correlation coefficient. Based on these metrics, a sensitivity analysis was conducted to find optimal frequency bands and σ values, which involved testing multiple frequency positions and bandwidths to identify those yielding the highest correlations with rainfall rate, as well as evaluating a range of percentile-based threshold values to minimize detection errors. Given the lack of consensus in the existing literature regarding which portions of the acoustic spectrum contain the most relevant rainfall signatures, especially in real-world scenarios, this analysis represents an effort to evaluate frequency-dependent sensitivity, as detailed in Section 3.

The sensitivity tests were carried out by testing a wide range of frequency bands and percentile values. An equal number of events (seven) was selected for each site, based on the location with the fewest available events (Chavascal). To ensure comparability, events from the larger datasets were selected based on their total rainfall, ensuring they match as closely as possible the magnitude of the Chavascal events. For each event, the correlation between the proposed metric and rain gauge measurements was calculated individually, and the final correlation reported for each location corresponds to the mean of these event-wise correlations.

A final validation step evaluates the cross-site generalization of the proposed approach. A single frequency window is selected based on the sensitivity test results, which exhibit a strong correlation to rainfall intensity across multiple sites. To ensure comparability, an equal number of rainfall events is selected for each dataset. Correlations between the proposed metric and rainfall are first calculated at the rain gauge resolution (e.g., mm/5min for most datasets, mm/2.5 min for Abidjan), and the resulting values are then averaged over each rainfall event to obtain a mean event-wise correlation for each site.

3 Results and discussion

The distribution of on-site rainfall measurements, along with corresponding audio recordings, is shown in Fig. 4. Data points (y-axis) are displayed on a logarithmic scale to accommodate the large number of low-intensity measurements (single or double-tip). Values above 20 mm h^{-1} are aggregated to improve visibility. In the central Amazon datasets, low-intensity rainfall (2-4 mm h^{-1}) represents an average of 62% of measurements, compared to 59% in UECE, 75% in ABJ (due to the rain gauge resolution of 0.5 mm), and 90% in the TLS-1,2 datasets. High-intensity rainfall (> 20 mm h^{-1}) is rare across all locations, accounting for roughly 5% of measurements in the central Amazon, 4% in UECE, 3% in ABJ, and only 0.3% in TLS.

https://doi.org/10.5194/egusphere-2026-3457
Preprint. Discussion started: 18 August 2026

3.1 Rainfall data analysis

The distribution of on-site rainfall measurements, along with corresponding audio recordings, is shown in Figure 4. Data points (y-axis) are displayed on a logarithmic scale to accommodate the large number of low-intensity measurements (single or double-tip). Values above 20 mm h^{-1} are aggregated to improve visibility. In the central Amazon datasets, low-intensity rainfall (2-4 mm h^{-1}) represents an average of 62% of measurements, compared to 59% in UECE, 75% in ABJ (due to the rain gauge resolution of 0.5 mm), and 90% in the TLS-1,2 datasets. High-intensity rainfall (> 20 mm h^{-1}) is rare across all locations, accounting for roughly 5% of measurements in the central Amazon, 4% in UECE, 3% in ABJ, and only 0.3% in TLS.

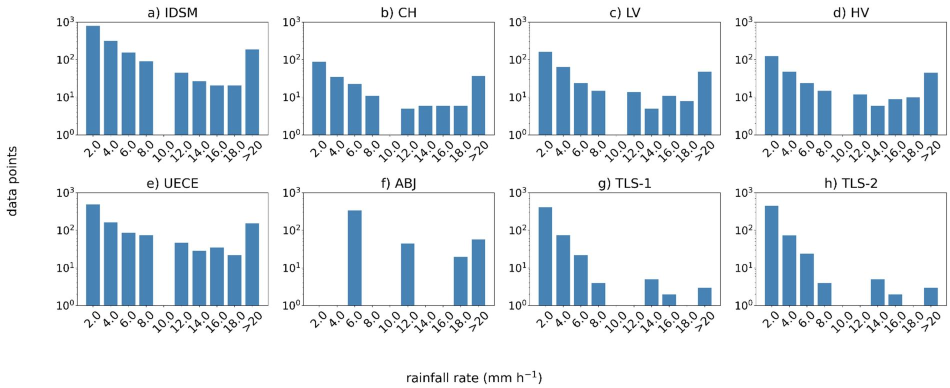

Figure 4: Rainfall data distribution for each dataset.

Event counts vary substantially across locations (see Table 1), ranging from seven events in the CH dataset to over fifty in the IDSM, reflecting differences in data availability. Across most sites, rainfall event durations are on the order of a few hundred timesteps (Fig. 5a), with mean durations ranging 1.2 hours (ABJ) to 2.9 hours (UECE). In comparison, total rainfall per event shows less variability among tropical regions, with mean event-wise accumulated rainfall generally ranging between approximately 17 mm in IDSM and 33 mm in ABJ, and maximum values rarely exceeding 100 mm (Fig. 5b). Events at TLS are characterized by lower accumulated rainfall, around 7 mm; this is consistent with its mid-latitude location, where precipitation is more frequently associated with large-scale, stratiform systems that produce weaker but persistent rainfall. The remaining sites are located in tropical regions, where rainfall is predominantly convective, resulting in more intense events.

https://doi.org/10.5194/egusphere-2026-3457
Preprint. Discussion started: 18 August 2026

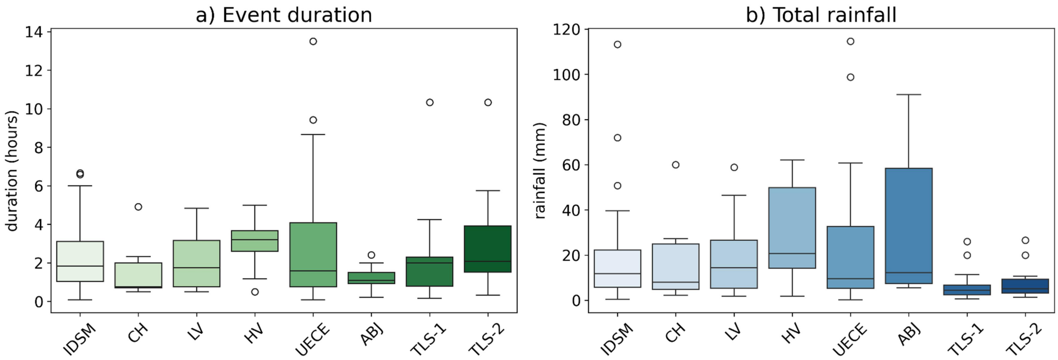

Figure 5: Boxplots representing event duration (a) and total rainfall (b) for each dataset, considering an MIT of 3 hours and a minimum of 6 timesteps of consecutive rain gauge measurements. In each boxplot, the horizontal line represents the median event duration or total rainfall, lower and upper bounds indicate the interquartile range, and the circles represent outlier rainfall events.

3.2 Sound data analysis

Although the acoustic signals across the study regions display a high variability, for the sites located in the central Amazon region (IDSM, CH, LV, and HV), a consistent pattern emerges (Fig. 6): rainfall produces more distinct acoustic signatures at lower frequencies (up to approximately 3 kHz), while considerable overlap between wet and dry conditions is observed at higher frequencies, which may be attributed to the interference of bioacoustic signals, that tends to dominate the higher-frequency bands (Fig. A1).

For the ABJ and TLS-1,2 datasets, wet periods are characterized by lower spectral variability, as indicated by narrower interquartile ranges. However, ABJ shows a more pronounced difference between wet and dry PSD values, TLS-1 exhibits an overlap between conditions at lower frequencies (approximately up to 1 kHz), whereas TLS-2 dry and wet conditions are closer together.

https://doi.org/10.5194/egusphere-2026-3457
Preprint. Discussion started: 18 August 2026

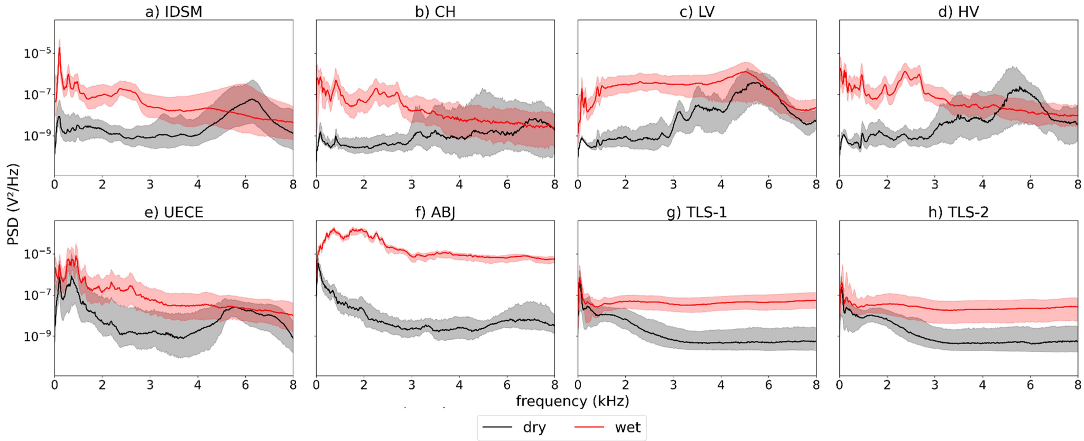

Figure 6: Power Spectrum Density of acoustic signals during wet (red) and dry (blue) conditions across study sites, the shaded area represents the interquartile range, and the solid line represents the median.

3.3 Sensitivity tests

Existing studies indicate that rainfall-related acoustic energy can be detected across a range of frequency bands; however, there is no clear consensus in the literature regarding an optimal frequency window for audio-based rainfall estimation. Reported approaches span both narrow and broad spectral ranges. For instance, Xavier et al. (2024) found a suitable window between 1.6 and 2.7 kHz, while Gaucherel & Grimaldi (2015) focused on a narrower band within 1.7 to 2.1 kHz. Bedoya et al. (2017) reported two distinct frequency windows for PSD-based rainfall detection, one from 0.6 to 1.2 kHz and another from 4.4 to 5.6 kHz. In contrast, Brown et al. (2019) detected a higher frequency window, between 6 and 8 kHz.

Given this variability and our diverse datasets, we adopted a broader frequency window spanning 0 to 5 kHz for our sensitivity tests, which encompasses most of the ranges previously identified in the literature. This choice is motivated by the substantial overlap at higher frequencies between dry and wet signatures observed in the Amazon and UECE datasets (Fig. 6). The selected range is further supported by the work of Hwang et al. (2024), who demonstrated the presence of rainfall signatures within this band using an acoustic recorder specifically built for attenuating ambient noise in rainy environments.

Optimization results are presented in two forms: (1) a correlation analysis using sliding frequency windows with varying widths and starting points; and (2) correlation and error estimates (Eq. 4) computed using a fixed 200 Hz window while varying the threshold parameter (σ). While computing the error metrics, previously defined as the weighted mean of false positives and false negatives, the proposed approach initially exhibited a relatively high false positive rate when evaluated strictly against rain-gauge measurements. However, manual inspection of the corresponding audio recordings

https://doi.org/10.5194/egusphere-2026-3457
Preprint. Discussion started: 18 August 2026

revealed the presence of audible rainfall in a substantial fraction of these cases. This may be explained by two factors: (1) limitation of rain gauge sampling; the metric may be able to capture the true intermittency of rainfall, a characteristic previously reported in audio-based methods for rainfall monitoring (Dunkerley, 2020); or (2) the presence of a forest canopy may introduce acoustic persistence after the cessation of measured rainfall, as residual dripping continues to produce rainfall-like sounds, which turns it into a source of error.

To account for this, an additional adjusted error metric is introduced to allow for a more consistent assessment: all audio files associated with the rainfall events were manually labeled as wet or dry based on inspection. Instances in which the proposed metric exceeded the threshold value and the rain gauge recorded no precipitation were re-evaluated: if the audio segment was labeled as wet, the detection was not considered a false positive.

Testing different frequency windows on rainfall events from the IDSM, CH, LV, and HV datasets and calculating their respective correlations (Fig. 7) reveals a consistent pattern across the study region, with two prominent frequency bands exhibiting higher correlation values. The first band, between 0.1 and 1 kHz, shows the highest correlations for the IDSM and CH datasets, with values of approximately 0.8 and above. A second band, from 1.7 to 2.7 kHz, exhibits the strongest correlations in the HV dataset, around 0.85. For the LV dataset, correlations are comparatively more homogenous across both bands. Across all sites, correlations tend to decrease at frequencies above 2.7 kHz. A drop in correlation is observed between 1 and 1.6 kHz for both IDSM and HV. The reason for this pattern is technophonic interference (Fig. B1), such as boat engines and machinery. This effect is less evident in the LV and CH datasets due to their distance from the river.

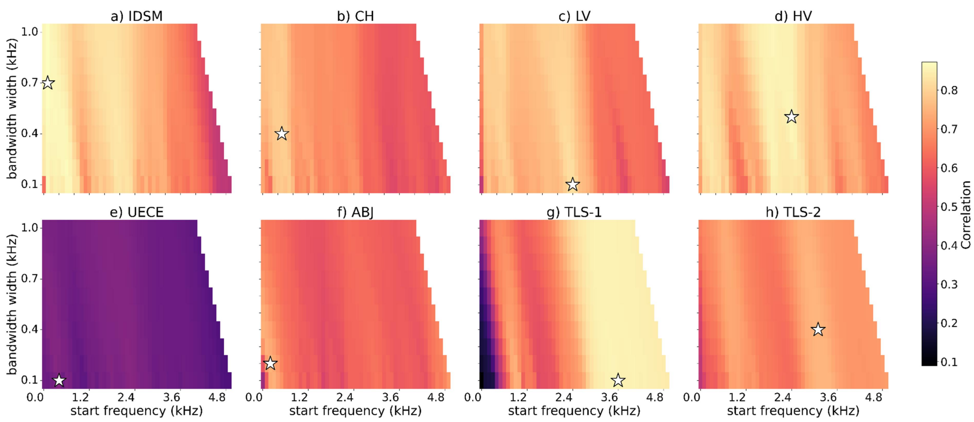

Figure 7: Heatmaps displaying the correlation values associated with different frequencies for the eight studied datasets; a star-shaped marker indicates the region with the highest correlation.

https://doi.org/10.5194/egusphere-2026-3457
Preprint. Discussion started: 18 August 2026

These findings are partially consistent with the previous studies conducted in tropical forest environments (Bedoya et al., 2017; Gaucherel & Grimaldi, 2015; Xavier et al., 2024). Xavier et al. (2024) which identified strong rainfall acoustic signals primarily within low-frequency bands. In particular, the lower frequency identified by Bedoya et al. (2017) of 0.6 to 1.2 kHz aligns well with the stronger correlations observed in the Amazonian sites (Fig. 7a to 7d). In contrast, the higher frequency of 4.4 to 5.6 kHz reported by the same authors does not yield comparable results. However, this frequency range shows improved performance for the TLS datasets (Fig. 7g and 7h), indicating that the relevance of higher-frequency rainfall signatures is likely site-dependent and influenced by local acoustic and environmental conditions.

For these datasets, the proposed metric reliably distinguishes wet from dry periods (Fig. 8a to 8d), with a threshold between 0.97 and 0.98 providing the most consistent results. Generally, performance decreases (higher error rate) at frequencies above 2.7 kHz, while the lower part of the spectrum remains the most informative one. The shaded areas of the error and the adjusted error display similar patterns. However, adjusted error values are considerably lower for the LV and CH datasets.

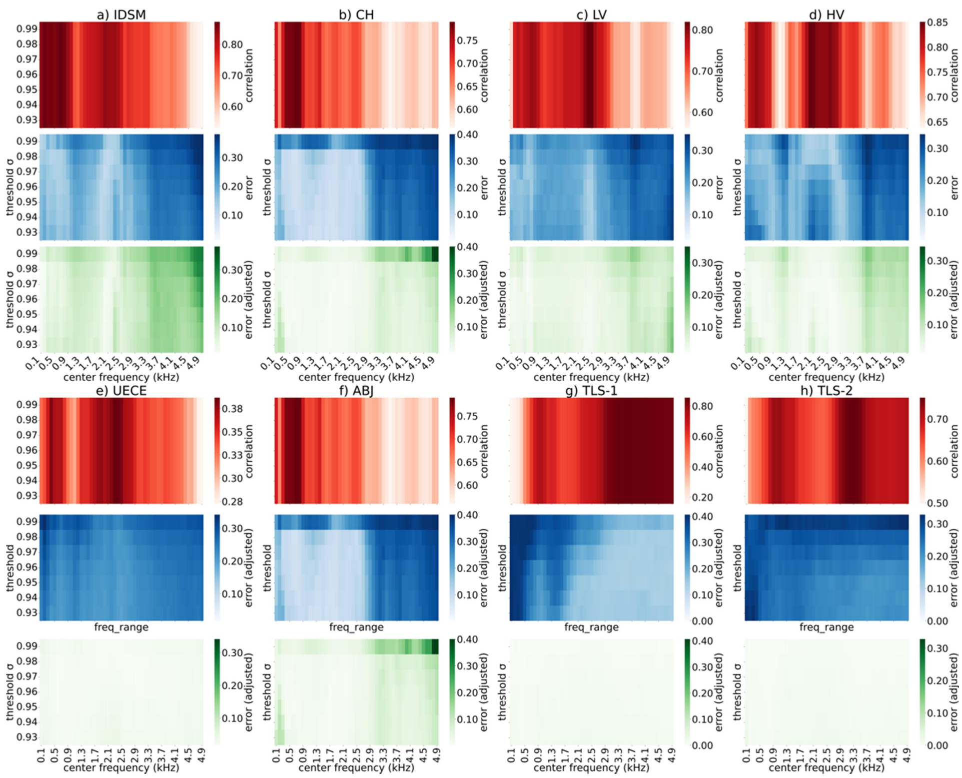

https://doi.org/10.5194/egusphere-2026-3457
Preprint. Discussion started: 18 August 2026

Figure 8: Sets of correlation (first and fourth rows), error (second and fifth rows), and adjusted error (third and sixth rows) heatmaps for the eight studied datasets. Darker (lighter) colours indicate regions of best (worst) performance in the correlation (error) plots.

For the UECE dataset, the correlation between the proposed metric and rainfall intensity is low (around 0.3) across the entire spectrum (Fig. 7e). The pattern of variation resembles other datasets, with higher correlation at lower frequencies, a decrease between 1 and 1.6 kHz, an increase afterwards, and a drop above 2.8 kHz. Since this recorder is the only one installed in an open-air environment, without a canopy or roof above it, this suggests that some structure is needed to amplify raindrop sounds and strengthen the correlation. Additionally, adjusted error values are lower than for other datasets (Fig. 8e), indicating that while the metric is not suitable for tracking rainfall intensity at this site, it can still capture the timing and intermittency of rainfall. Moreover, these results also highlight that residual droplets after rain cessation, influenced by the presence of a canopy, can be a source of error.

Similarly, the recorder in Abidjan is located in a semi-urban area and lacks a forest canopy. The main distinction with the previous setup is the presence of a roof-like structure positioned above the recorder. This may explain the higher correlation values, up to around 0.75 (Fig. 8f), although these remain lower than those observed in the Amazonian datasets. The highest correlations occur at a narrower window within lower frequency bands (around 0.3 to 0.8 kHz). Correlation values increase again at higher frequencies (above 4.6 kHz), and error detection performs best with thresholds close to 0.97 (Fig. 8f), with a decrease in performance at lower threshold values.

Unlike other locations, the TLS datasets exhibit their lowest correlation values in the lower part of the spectrum (Fig. 7g and 7h), although this is more notable for the TLS-1 dataset. At frequencies above 2.8 kHz, the correlation between the proposed metric and rainfall rate becomes comparatively homogenous, with values around 0.8 across a broad spectral range for the TLS-1 dataset, indicating a different response of the metric in this mid-latitude setting. Additionally, rainfall detection performance improves for higher threshold values (Fig. 8g).

3.4 Cross-site generalization

This analysis consisted of testing multiple frequency windows within the three most promising spectral bands (0.1 to 1.0 kHz, 1.7 to 2.7 kHz, and 2.8 to 4.0 kHz) across seven rainfall events from the remaining datasets. The number of events was determined by the smallest number of rainfall events available (CH dataset). To ensure comparable number of events across datasets, these seven events were randomly selected, prioritizing events with total rainfall amounts closest to those observed in the CH dataset. The occurrence of multiple optimal bands suggests that rainfall-related acoustic signatures interact differently according to site-specific sound sources, rather than being confined to a universal optimal window. Table 2 summarizes the optimal frequency window for each dataset. For the IDSM, CH, LV, HV, and ABJ datasets, lower-frequency bands generally dominate, with a common overlap between 0.5 and 0.8 kHz for the Amazonian sites; however, for

https://doi.org/10.5194/egusphere-2026-3457
Preprint. Discussion started: 18 August 2026

both LV and HV, combining this low-frequency range with a mid-frequency window (1.8 to 2.5 kHz) yields the strongest correlations. On the other hand, for the TLS datasets, the best results are obtained when considering higher frequency bands. The UECE dataset shows a similar tendency toward stronger correlations in the low-frequency range (0.1-0.4 kHz); however, the maximum correlation obtained (0.39) is not statistically significant.

Selecting a single frequency window applicable across all tropical locations requires some loss of performance at the individual-site level. Among the tested bands, the 0.2 to 0.5 kHz window is the only range for which all five tropical region datasets achieved a mean event-wise correlation greater than 0.7; therefore, it was selected as the final frequency band for the cross-site analysis, which included the IDSM, CH, LV, HV, and ABJ datasets. In comparison, the optimal window chosen for the TLS datasets that fits this criterion is 3.2-3.5 kHz. This relationship between rainfall intensity and energy distribution in the low-frequency range (0-1 kHz) has also been documented in a recent work by Wang et al. (2026), where the authors found that low-frequency energy accounts for approximately 83% of the total acoustic signal during rainfall events. Their analysis further showed that, although low frequencies remain dominant, the relative contribution of mid-frequency components increases with rainfall intensity. It is worth noting, however, that the recorder used in their study was deployed in an acoustically controlled environment with minimal external interference, whereas our recordings were obtained under more heterogeneous conditions.

Table 2: Best-performing frequency bands for each dataset.

Site	Best band(s) (kHz)	Mean correlation
IDSM	0.6 to 0.8	0.87
CH	0.5 to 0.9	0.80
LV	0.5 to 0.7 and 1.8 to 2.0	0.82
HV	0.5 to 0.7 and 2.3 to 2.5	0.85
UECE	0.1 to 0.4	0.39
ABJ	0.2 to 0.4	0.75
TLS-1	3.6 to 3.8	0.85
TLS-2	3.2 to 3.4	0.76

Across all datasets, there is a mostly monotonic increase in median metric values from light to violent rainfall (Fig. 9), indicating that the proposed metric scales well with rainfall intensity. For IDSM, CH, LV, and HV, the interquartile ranges show less overlapping between non-adjacent classes, and the increase in medians and upper quartiles supports the sensitivity of the metric to increasing precipitation intensity. The UECE dataset also displays a similar pattern; however, it presents more dispersion and overlapping among categories, consistent with the lower correlations previously observed. For ABJ, light rainfall samples are not available due to the rain gauge resolution, which limits classification at the lowest intensities; additionally, a high overlap between heavy and violent rainfall can be observed. In the TLS datasets, only one

https://doi.org/10.5194/egusphere-2026-3457
Preprint. Discussion started: 18 August 2026

violent rainfall event was recorded, which limits this analysis; nevertheless, the proposed metric still shows a clear increase from light to heavy rainfall.

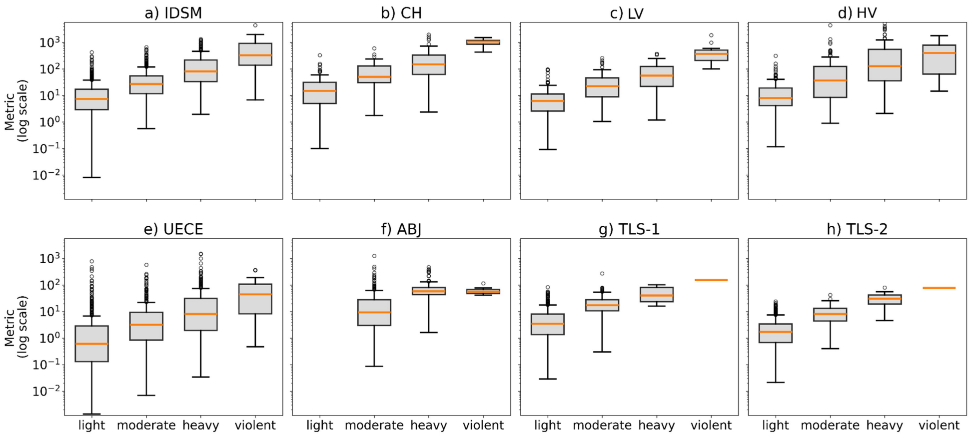

Figure 9: Boxplots of the proposed metric (on a log scale) across each dataset using optimal frequency window (0.2-0.5 kHz for the tropical datasets, 3.2-3.5 kHz for the TLS datasets), for different rainfall intensity classes (light, moderate, heavy, and violent). In each boxplot, the horizontal line indicates the median and interquartile range, and the circles are individual outliers. Note that the light rainfall category is absent from the ABJ dataset (f) due to rain gauge resolution.

The resulting mean correlation between the proposed acoustic metric and total rainfall for each of the seven events is shown in Fig. 10a. Due to the low correlation values, the UECE dataset was not included in this analysis. Overall, strong correlations are obtained across all datasets, with mean values ranging from 0.61 for ABJ and 0.84 for HV, indicating a consistent relationship between low-frequency acoustic energy and accumulated rainfall across distinct environments. Most events are grouped at moderate to high correlation values, mostly independent of total rainfall amount. However, four events exhibit noticeably lower correlations; three of them (for CH, IDSM, and HV) are associated with low accumulated rainfall, while one (for ABJ) is associated with a total rain of more than 80 mm. These low correlation values are mainly associated with temporal misalignment between the proposed metric and rain gauge measurements, rain gauge malfunction, local rainfall variability due to spatial separation between the recorder and the gauge, and short-lived rainfall events (Fig. C1).

Figure 10b contains the mean error values obtained using the optimal frequency window for each dataset as a function of the percentile-based threshold σ used for rainfall detection. When relying solely on rain gauge measurements as ground truth, the gauge-based error stabilizes at values around 0.2 for thresholds between 0.98 and 0.99. The adjusted error, which accounts for manual audio-based validation, exhibits similarly low values over a wider range of thresholds, but increases at a threshold of 0.99. Based on these results, a threshold value of 0.98 represents a reasonable compromise, yielding a mean error of approximately 0.02 when adjusted using manual audio inspection.

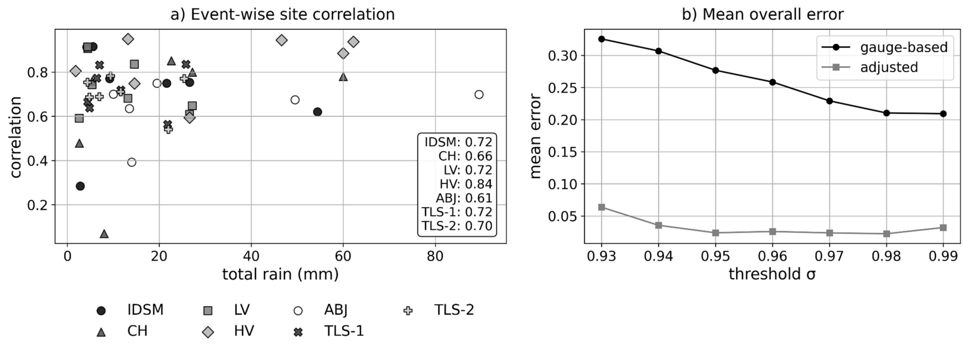

Figure 10: Event-wise correlation (a), values inside the plot correspond to the overall mean correlation values; and overall mean errors (b) across multiple sites using the optimal frequency window (0.2-0.5 kHz and 3.2-3-5 kHz for the TLS datasets) for different threshold values.

The low correlation values obtained with the 0.2-0.5 kHz band in the TLS datasets are mostly associated with wind and jet engine interferences. At TLS-1, wind-induced fluctuations strongly affect the metric performance at lower frequencies, while at TLS-2, the vegetation partially attenuates this effect, yielding higher correlations for some of the events (Fig. D1). However, several low-correlation cases for the TLS-2 dataset can be linked to jet engine noise, which dominates the frequencies below ≈ 2 kHz (Fig. D2), masking rainfall signals. When these noise-contaminated periods are excluded, the mean correlation of the optimal frequency band becomes comparable to that obtained with the higher frequency window. These results suggest that, if wind and technophonic noises are absent or filtered out; the 0.2-0.5 kHz band could also be suitable for the TLS datasets.

3.5 Potential applications and future perspectives

Although the proposed metric does not provide a direct estimate of instantaneous rainfall rate, it displays a strong correlation with accumulated precipitation across all locations. At the same time, its amplitude differs substantially between sites, indicating that local elements such as canopy presence and density play a significant role in the metric's scaling, which limits the development of a general physical equation for rainfall rate estimation. Similar observations have been reported in previous studies (Peleg et al., 2023), suggesting that acoustic measurements can provide valuable information on rainfall duration and magnitude, and may serve as a complementary source of information when merged with other tools. A potential

https://doi.org/10.5194/egusphere-2026-3457
Preprint. Discussion started: 18 August 2026

approach to achieve this is the use of a local calibration factor: when scaled using total rainfall over a given period (e.g., satellite precipitation products), the acoustic metric may be used to infer the rainfall variability within that interval, providing data that remains valuable even in the absence of conventional ground-based measurements.

During the data analysis, we identified a period during which the rain gauge inside the RDSM malfunctioned; interestingly, the proposed acoustic metric also indicated a potential rain event during this interval. To estimate the total rainfall for this period, we used the GPM IMERG Late Precipitation product, which provided an independent reference for the accumulated precipitation. Using this total rainfall, we computed a local scaling factor based on the ratio between the total estimated precipitation from GPM and the sum of the metric values that exceeded the 0.98 percentile of the dry-weather baseline, with total rain values set to zero for metric values below the threshold. This enables the conversion of raw acoustic metric values into an estimated high-resolution time series (Fig. 11). The increase of the acoustic rainfall signal coincides with the arrival of colder cloud-top temperatures over the LV site, consistent with deeper convective activity observed in the GOES-16 imagery. However, an initial peak in the metric, around 19:00 (local time), is unrelated to precipitation, and manual inspection of the audio revealed wind-related sounds. This issue should be addressed in future work, as mitigating this effect would increase methodological performance across all sites.

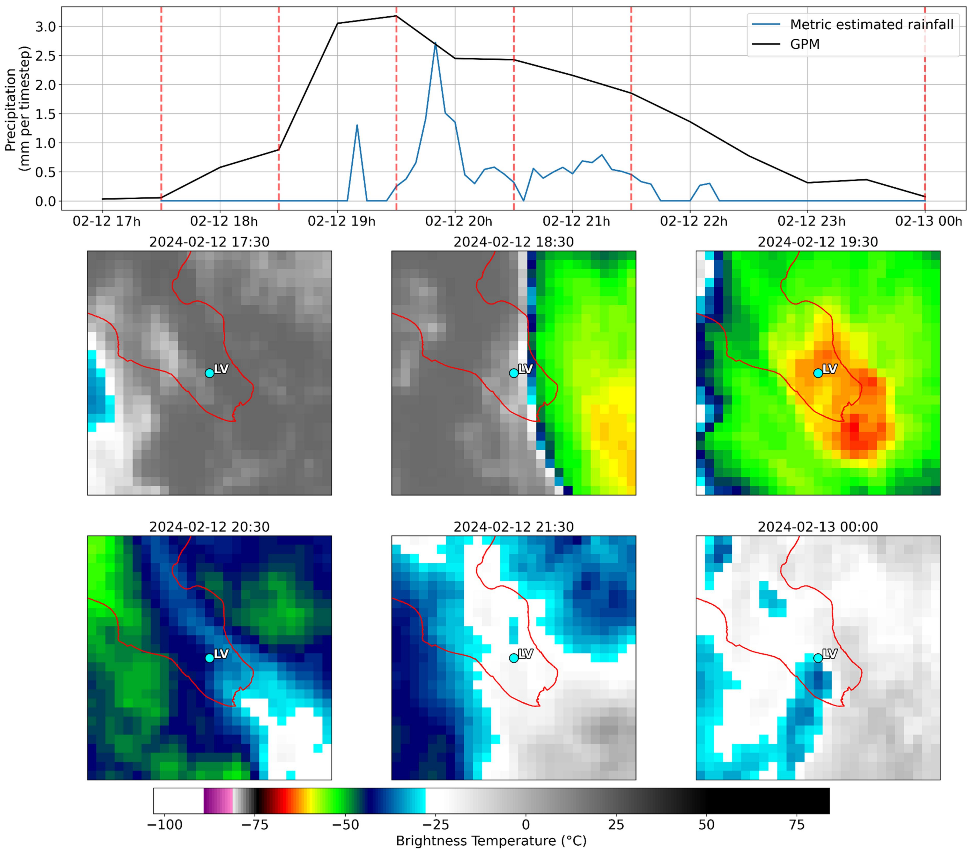

Figure 11: Time series of a rainfall event (top panel) showing precipitation estimates from the acoustic metric (blue) and GPM-IMERG observations (black). Vertical dashed red lines indicate timestamps of GOES-16 satellite images (bottom rows), using Band 13 (10.3 µm). The satellite images show brightness temperature over the Low Várzea (LV) recorder (cyan marker), inside the RDSM.

These results reinforce that the proposed acoustic baseline method performs consistently across diverse climatic settings, including tropical and temperate environments. Our proposed metric exhibits strong temporal coherence with rainfall variability, allowing for cross-site application despite differences in vegetation structure and rainfall climatologies. However, background noises, particularly wind-related and from machinery or aircraft engines, remain a challenge for

https://doi.org/10.5194/egusphere-2026-3457
Preprint. Discussion started: 18 August 2026

improving cross-site generalizability. Its minimal data requirements (relying on a reference period of known dry weather) make our approach suitable for low-cost rainfall monitoring, particularly in remote or underrepresented regions.

A limitation of this study is that the analysis is mainly focused on correlation rather than the direct retrieval of rainfall rate. Future work should therefore further explore the derivation of local, site-specific relationships between the proposed metric and rainfall intensity, rather than assuming a universal physical relationship. Moreover, additional research is needed to better understand how the methodology performs in an open-air environment. In this study, the UECE dataset was excluded from our more detailed analysis due to its low correlation values, and further investigation is needed into different approaches for recovering rainfall-related information from its acoustic data. Previous studies suggest that the use of simple additions, such as a plastic shelter above the recorder, may provide a viable way for performance improvement for sensors placed in an open-air environment (Avanzato et al., 2019; Wang et al., 2023). Additionally, future efforts will be dedicated to detailed data standardization and annotation of all collected datasets, enabling public access to the curated audio data. Annotated public datasets in this field remain scarce, which limits the development of this still underexplored research area.

4 Conclusions

The use of sound-based methods for rainfall estimation has been gaining attention in recent years. However, most existing approaches rely on model training, lack cross-site validation, or are based on simulated rainfall, limiting their practical applicability. The present study demonstrated the potential of a simple, training-free acoustic framework for rainfall monitoring under real-world conditions. While acoustic methods have previously been investigated for rainfall estimation, this study is, to our knowledge, the first to evaluate this approach across multiple environments and experimental settings. We adapted an existing methodology, previously employed with signals received from commercial microwave links, for the first time to an audio-based framework across eight datasets spanning tropical and mid-latitude environments. Despite the diversity of sites, the proposed methodology exhibited consistent performance, yielding a mean correlation of 0.71 with accumulated rainfall across all locations and higher than 0.9 in best-case scenarios. Rainfall detection based on a percentile threshold of the dry-weather baseline showed a stable performance, with a threshold value of 0.98 providing the best results, yielding an error of 0.2 relative to rain gauge measurements, which was further reduced to 0.02 when adjusted using manual audio inspection.

The analysis revealed that low-frequency bands (0.2 to 0.5 kHz) are particularly effective for capturing rainfall variability in tropical environments, especially when a canopy or surface is present for amplifying raindrop impacts. In contrast, at the mid-latitude sites, correlations at low frequencies were more strongly influenced by wind and technophonic (e.g., aircraft engines) noise, while higher-frequency windows (3.2 to 3.5 kHz) provided more consistent results. These findings underscore the importance of site-specific considerations when selecting optimal frequency windows. A key strength of this work lies in its evaluation of rainfall acoustics under real-world conditions, where biophonic,

https://doi.org/10.5194/egusphere-2026-3457
Preprint. Discussion started: 18 August 2026

anthropophonic, and geophonic sources coexist. Furthermore, the analysis was done on a diverse set of locations, with distinct climatologies, including tropical and temperate regions, forest and semi-urban environments. Given that the current literature on sound-based rainfall estimation remains limited, and cross-site validation even more so, demonstrating consistent performance across multiple, geographically and climatologically distinct locations represents a step toward practical applicability.

Appendix A: Baseline acoustic conditions

Figure A1 illustrates the point highlighted in Figure 2 regarding the dry weather baseline daily cycle for the IDSM dataset. The top spectrogram shows increased biophonic activity during nighttime hours (18:30), caused by nocturnal animals and insects. Calls from different animals dominate the spectra between 2-10 kHz, with a cicada call starting around the 10-s mark being particularly prominent. The bottom spectrogram, recorded at 15:00, also shows bioacoustic activity, but it is much less pronounced.

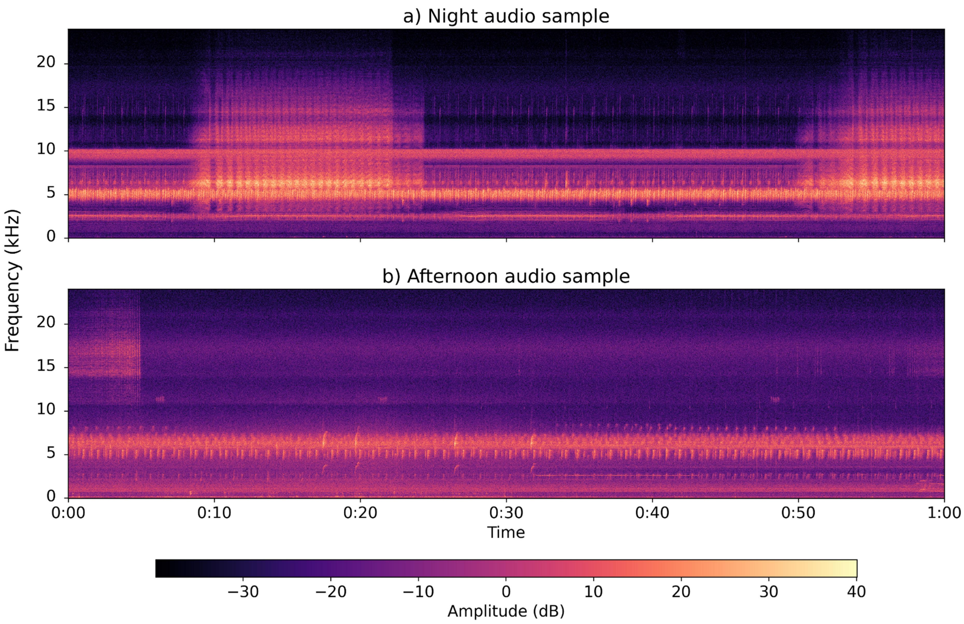

Figure A1. Spectrograms from two audio samples showing different biophonic activity, at night (a) and afternoon (b), for the IDSM dataset.

https://doi.org/10.5194/egusphere-2026-3457
Preprint. Discussion started: 18 August 2026

Appendix B: Sources of error and signal interference

Figure B1 depicts the overlap of audios containing rainfall (wet) and engine (technophonic) sounds at the 1-1.8 kHz, which decreases the correlation of the proposed metric with rainfall rate, effect visible on Figures 8 and 9 for the IDSM dataset. Due to its proximity to the river, the same effect is observed for the HV dataset.

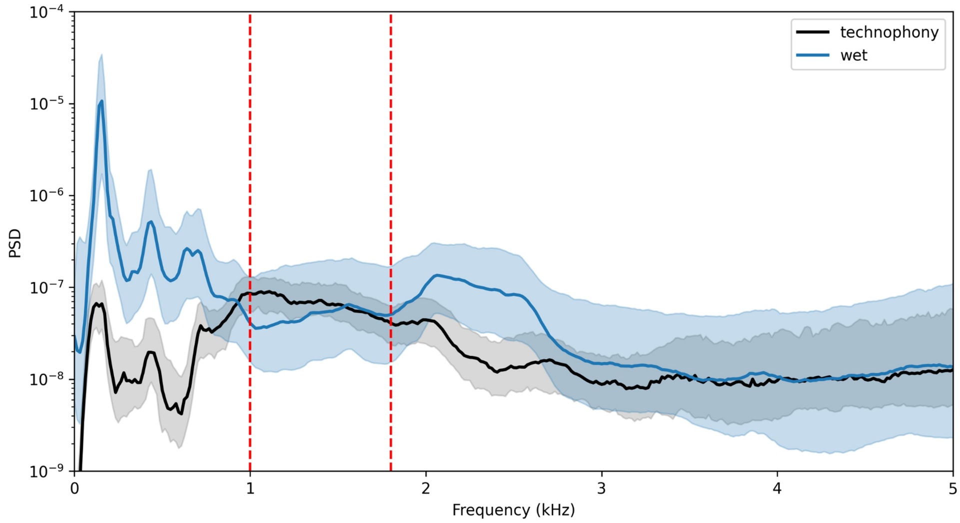

Figure B1. Median PSDs of wet (blue) and technophonic (black) audios and their interquartile range (shaded area) for the IDSM dataset. Dashed red lines indicate the region between 1-1.8 kHz.

Appendix C: Low correlation rainfall events analysis

Figure C1 presents the time series of the rainfall events associated with the lowest correlation values, starting two hours before rainfall onset to highlight pre-event conditions. The rainfall event in the IDSM dataset (Fig. C1a) is short-lived and characterized by low accumulated rainfall (2.8 mm). The reduced correlation arises from a temporal misalignment between the proposed metric and rain gauge measurements. While the rain gauge records a single main peak of 0.6 mm, the metric exhibits three distinct peaks; the third peak, observed at 20:30, coincides with a rain gauge measurement of 0 mm. However, manual inspection of the corresponding audio confirms the presence of rainfall. This suggests a timing offset in the rain gauge records rather than a failure of the metric, which still captures the onset and cessation of the event.

Figure C1b shows the event with the lowest correlation across all analyzed datasets (0.29). This event is also short-lived, with two rainfall peaks of approximately 2 mm, separated by a period during which the rain gauge records around 1 mm of rainfall. Audio inspection during this interval reveals only faint rainfall sounds, which may be attributed to the spatial

https://doi.org/10.5194/egusphere-2026-3457
Preprint. Discussion started: 18 August 2026

separation between the recorder and the rain gauge, resulting in local variability. A third and more pronounced peak appears after the event has ended (around 18:00); the associated audio indicates bioacoustic activity very near the recorder, which constitutes a clear source of error for the proposed metric in this case. Figure C1c (HV dataset) shows evidence of rainfall occurring before the defined event onset, which is constrained by the criterion of 6 timesteps of consecutive rain gauge measurements. Based on this definition, the total accumulated rainfall is 1.8 mm. The proposed metric captures the event variations until approximately 20:35. Audio inspection again indicates the presence of rainfall sounds after the rain gauge ceased recording precipitation. Given the proximity between the recorder and the rain gauge, local rainfall variability is unlikely, and it's unclear whether this discrepancy is caused by rain gauge malfunction. Finally, the event in the ABJ dataset (Fig. C1d) corresponds to a longer event, approximately two hours in duration, with accumulated rainfall of 91 mm. The proposed metric correctly identifies both the beginning and the end of the event. As shown in Fig. C1a, the lower correlation values primarily result from temporal misalignment between the metric and rain gauge measurements rather than an inability to detect rainfall occurrences.

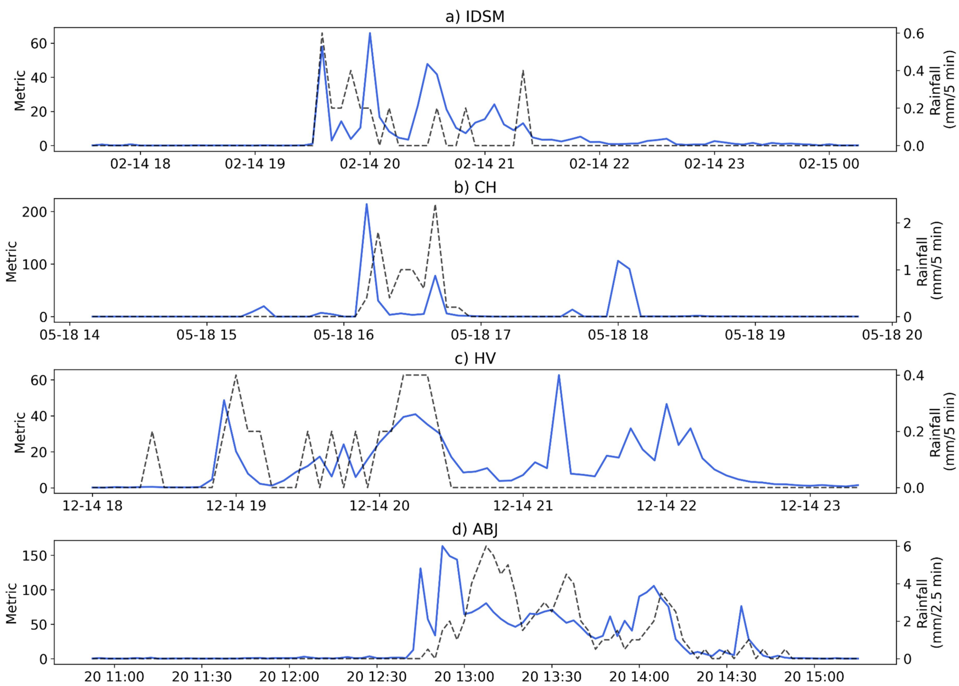

https://doi.org/10.5194/egusphere-2026-3457
Preprint. Discussion started: 18 August 2026

Figure C1. Time series of the rainfall events associated with the lowest correlation values between the proposed metric (blue) and rainfall measurements (dashed black).

Appendix D: TLS site-specific analysis

In a separate analysis, we examine the performance of the proposed metric for the TLS datasets. Figure D1 shows a rainfall event recorded between 2025-11-06 07:05 and 2025-11-07 08:00. The top panels apply the metric within the low-frequency window (0.2 to 0.5 kHz). In contrast, the bottom panels use the frequency window identified as optimal for TLS (3.2 to 3.5 kHz). When the low-frequency window is applied to the TLS-1 dataset (Fig. D1a), the resulting correlation with rainfall rate is very low (r = -0.04); in contrast, the higher-frequency window yields a substantially higher correlation (r = 0.91). This poor performance of the low-frequency band at TLS-1 is associated with a meteorological factor that did not significantly affect the other datasets: wind. In mid-latitude regions, rainfall is primarily driven by the strong horizontal temperature gradients and enhanced wind activity, in contrast to tropical environments where convection and vertical instability are the main factors influencing rainfall. The influence of wind (red dots on Fig. D1) is evident from pronounced metric fluctuations preceding the onset of rainfall measured by the gauge, particularly around 00:00. While the use of the higher-frequency window considerably attenuates wind effects, a variability is still present, indicating that wind may still act as a source of error for rainfall detection.

Figure D1b presents the same results for the TLS-2 dataset, located only a few meters away but within denser vegetation and under a lower canopy. In this configuration, the surrounding vegetation acts as a barrier, mitigating wind-induced fluctuations. As a result, the low-frequency window performs comparably to the higher band, both yielding correlations of approximately 0.85 for the illustrated event. This contrast between TLS-1 and TLS-2 highlights a strong influence of local vegetation structure on the proposed metric.

https://doi.org/10.5194/egusphere-2026-3457
Preprint. Discussion started: 18 August 2026

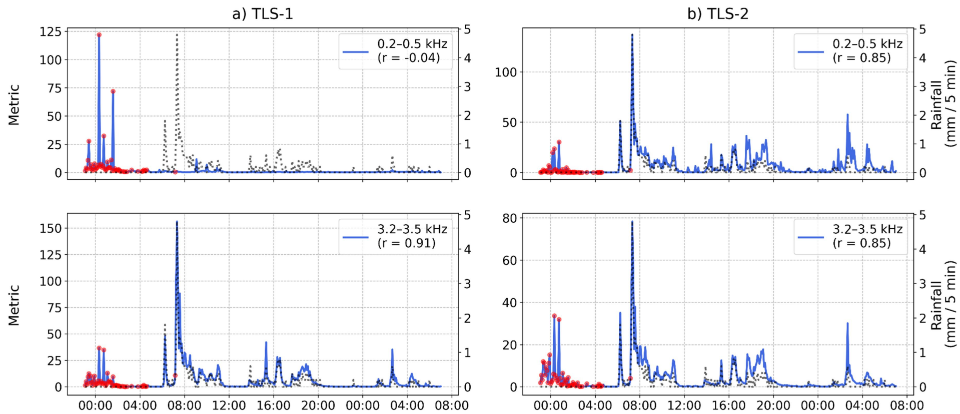

Figure D1. Time series of a rainfall event of the TLS datasets using the optimal frequency window of 0.2-0.5 kHz (top) and the TLS-specific frequency window 3.2-3.5 kHz (bottom). Red markers indicate time steps when wind speed exceeded 2 m s⁻¹.

As shown in Fig. D2, the low-frequency band (0.2 to 0.5 kHz) yields high correlation values for the TLS-2 dataset. However, when considering all rainfall events, the consistently best-performing window for this site corresponds to the higher-frequency band. To investigate this difference, we analyzed events for which the low-frequency band performed poorly (Figure D2). In these cases, wind speed shows limited influence on the metric, yet pronounced metric peaks unrelated to rainfall are observed.

Manual inspection of the audio corresponding to these peaks reveals the presence of jet engine noise, as illustrated by the spectrogram in the bottom panel of Fig. D2. This signal dominates the spectrum up to approximately 2 kHz, therefore degrading the correlation between the low-frequency metric and rainfall rate. Such interference is observed in three out of the seven analyzed events. When these periods are excluded, the mean correlation for the low-frequency band increases to 0.8, comparable to the value obtained using the higher-frequency window (0.78). This result suggests that the lower-frequency window identified for the other datasets may also apply to the TLS-2 dataset under conditions where background technophonic noise is filtered out or absent.

https://doi.org/10.5194/egusphere-2026-3457
Preprint. Discussion started: 18 August 2026

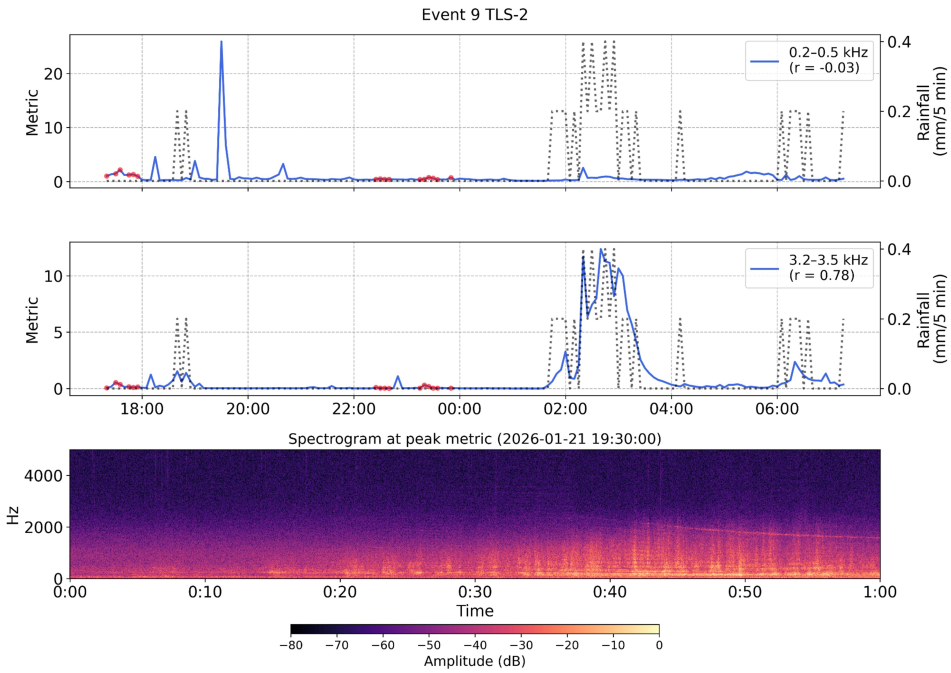

Figure D2. Time series from the TLS-2 dataset for a rainfall event occurring on January 21, 2026, between 02:20 and 09:05. The top panel shows the proposed metric computed within the 0.2 to 0.5 kHz frequency window, while the middle panel displays the metric values obtained using the 3.2 to 3.5 kHz window. Red markers indicate time steps when wind speed exceeded 2 m s^{-1}. The bottom panel presents the spectrogram of the audio segment corresponding to the maximum metric value in the top panel, which occurred on 21 January 21, 2026 at 19:30.

Author contributions

RSX ASF MG conceptualized the study. RSX, MK, and TGS collected the data. RSX curated the data. RSX, TFM, and MG performed the data analyses. ASF and TFM acquired the funding. RSX, TFM, and MG designed the methodology. RSX, ASF, TFM, and MG prepared the original draft. All authors reviewed and edited the manuscript.

Competing interests

The contact author has declared that none of the authors has any competing interests.

https://doi.org/10.5194/egusphere-2026-3457
Preprint. Discussion started: 18 August 2026

Code availability

An interactive Jupyter Notebook with simple code, used to calculate the proposed acoustic metric presented in the research https://doi.org/10.23708/UMPMKI. It also contains 16 datasets in the CSV format related to the 8 research sites and PSDs extracted from the rainfall events.

Disclaimer

Publisher's note: "Copernicus Publications remains neutral with regard to jurisdictional claims made in the text, published maps, institutional affiliations, or any other geographical representation in this paper. While Copernicus Publications makes every effort to include appropriate place names, the final responsibility lies with the authors. Views expressed in the text are those of the authors and do not necessarily reflect the views of the publisher."

Acknowledgements

The authors thank the Mamirauá Institute for Sustainable Development for the continuous efforts put into data collection and the Cearense Foundation for Meteorology and Water Resources (FUNCEME) for providing the Fortaleza rainfall data. The main author acknowledges the use of AI-assisted tools for spell-checking and language translation, the content and intellectual contributions remain the sole responsibility of the authors.

Financial support

CNPq for its financial support through grants 402661/2024-9 and 312471/2021-1.
Funding by Gordon and Betty Moore Foundation (Project "Advancing the understanding of methane emissions from tropical wetlands"), Fundação de Amparo à Pesquisa do Estado do Amazonas (FAPEAM), Secretaria de Estado de Desenvolvimento Econômico, Ciência, Tecnologia e Inovação (SEDECTI), and the Governo do Estado do Amazonas – EDITAL 003/ 2023 - PAINTER INFRA CT&I. The authors thank the State Secretariat for the Environment of the Amazonas State for the support in the research conducted at the Mamirauá Sustainable Development Reserve.

References

Adom, P. K. (2024). The socioeconomic impact of climate change in developing countries over the next decades: A literature survey. Heliyon, 10(15), e35134. https://doi.org/10.1016/j.heliyon.2024.e35134

https://doi.org/10.5194/egusphere-2026-3457
Preprint. Discussion started: 18 August 2026

Alkhatib, M. I. I., Talei, A., Chang, T. K., Hermawan, A. A., & Pauwels, V. R. N. (2024). Towards the development of a citizens’ science-based acoustic rainfall sensing system. Journal of Hydrology, 633, 130973. https://doi.org/10.1016/j.jhydrol.2024.130973

Alkhatib, M. I. I., Talei, A., Chang, T. K., Pauwels, V. R. N., & Chow, M. F. (2023). An Urban Acoustic Rainfall Estimation Technique Using a CNN Inversion Approach for Potential Smart City Applications. Smart Cities, 6(6), 3112–3137. https://doi.org/10.3390/smartcities6060139

Alvares, C. A., Stape, J. L., & Sentelhas, P. C. (2013). Ko¨ppen’s climate classification map for Brazil. Meteorol. Z.

Aquino, D. J., Eusebio, L. F., & Loresco, P. J. (2022). ANN-Based Classification of Rain Acoustic Sensor Data Using Modified Mel Frequency Cepstral Coefficients. 2022 IEEE 14th International Conference on Humanoid, Nanotechnology, Information Technology, Communication and Control, Environment, and Management (HNICEM), 1–6. https://doi.org/10.1109/HNICEM57413.2022.10109405

Avanzato, R., & Beritelli, F. (2020). An Innovative Acoustic Rain Gauge Based on Convolutional Neural Networks. Information, 11(4), 183. https://doi.org/10.3390/info11040183

Avanzato, R., Beritelli, F., Di Franco, F., & Puglisi, V. F. (2019). A Convolutional Neural Networks Approach to Audio Classification for Rainfall Estimation. 2019 10th IEEE International Conference on Intelligent Data Acquisition and Advanced Computing Systems: Technology and Applications (IDAACS), 285–289. https://doi.org/10.1109/IDAACS.2019.8924399

Beck, H. E., Zimmermann, N. E., McVicar, T. R., Vergopolan, N., Berg, A., & Wood, E. F. (2018). Present and future Köppen-Geiger climate classification maps at 1-km resolution. Scientific Data, 5(1), 180214. https://doi.org/10.1038/sdata.2018.214

Bedoya, C., Isaza, C., Daza, J. M., & López, J. D. (2017). Automatic identification of rainfall in acoustic recordings. Ecological Indicators, 75, 95–100. https://doi.org/10.1016/j.ecolind.2016.12.018

Brown, A., Garg, S., & Montgomery, J. (2019). Automatic rain and cicada chorus filtering of bird acoustic data. Applied Soft Computing, 81, 105501. https://doi.org/10.1016/j.asoc.2019.105501

Calvin, K., Dasgupta, D., Krinner, G., Mukherji, A., Thorne, P. W., Trisos, C., Romero, J., Aldunce, P., Barrett, K., Blanco, G., Cheung, W. W. L., Connors, S., Denton, F., Diongue-Niang, A., Dodman, D., Garschagen, M., Geden, O., Hayward, B., Jones, C., … Péan, C. (com Lee, H.). (2023). IPCC, 2023: Climate Change 2023: Synthesis Report. Contribution of Working Groups I, II and III to the Sixth Assessment Report of the Intergovernmental Panel on Climate Change [Core Writing Team, H. Lee and J. Romero (eds.)]. IPCC, Geneva, Switzerland. (First). Intergovernmental Panel on Climate Change (IPCC). https://doi.org/10.59327/IPCC/AR6-9789291691647

Capin, J. L. E., & Dimaunahan, E. D. (2023). Implementation of Neural Network Models Using Acoustic and Spectral Features for Rainfall Intensity Classification. 2023 4th International Conference on Industrial Engineering and Artificial Intelligence (IEAI), 23–29. https://doi.org/10.1109/IEAI59107.2023.00011

Chen, M., Wang, X., Wang, M., Liu, X., Wu, Y., & Wang, X. (2022). Estimating Rainfall from Surveillance Audio Based on Parallel Network with Multi-Scale Fusion and Attention Mechanism. Remote Sensing, 14(22), 5750. https://doi.org/10.3390/rs14225750

Chwala, C., Gmeiner, A., Qiu, W., Hipp, S., Nienaber, D., Siart, U., Eibert, T., Pohl, M., Seltmann, J., Fritz, J., & Kunstmann, H. (2012). Precipitation observation using microwave backhaul links in the alpine and pre-alpine region of Southern Germany. Hydrology and Earth System Sciences, 16(8), 2647–2661. https://doi.org/10.5194/hess-16-2647-2012

Dunkerley, D. (2008). Identifying individual rain events from pluviograph records: A review with analysis of data from an Australian dryland site. Hydrological Processes, 22(26), 5024–5036. https://doi.org/10.1002/hyp.7122

Dunkerley, D. (2020). Acquiring unbiased rainfall duration and intensity data from tipping-bucket rain gauges: A new approach using synchronised acoustic recordings. Atmospheric Research, 244, 105055. https://doi.org/10.1016/j.atmosres.2020.105055

Dunkerley, D. (2026). A New Device for Continuous, Real-Time Acoustic Measurement of Rain Inclination. Water, 18(4), 495. https://doi.org/10.3390/w18040495

Ferreira-Ferreira, J., Silva, T. S. F., Streher, A. S., Affonso, A. G., De Almeida Furtado, L. F., Forsberg, B. R., Valsecchi, J., Queiroz, H. L., & De Moraes Novo, E. M. L. (2015). Combining ALOS/PALSAR derived vegetation structure and inundation patterns to characterize major vegetation types in the Mamirauá Sustainable Development Reserve, Central Amazon floodplain, Brazil. Wetlands Ecology and Management, 23(1), 41–59. https://doi.org/10.1007/s11273-014-9359-1

Gaucherel, C., & Grimaldi, V. (2015). The Pluviophone: Measuring Rainfall by Its Sound. Journal of Vibration and Acoustics, 137(3), 034504. https://doi.org/10.1115/1.4029645

Guide to Meteorological Instruments and Methods of Observation. (2023). World Meteorological Organization.

Guo, H., Huang, H., Sun, Y.-E., Zhang, Y., Chen, S., & Huang, L. (2019). Chaac: Real-Time and Fine-Grained Rain Detection and Measurement Using Smartphones. IEEE Internet of Things Journal, 6(1), 997–1009. https://doi.org/10.1109/JIOT.2018.2866690

Hwang, S., Jun, C., De Michele, C., Kim, H.-J., & Lee, J. (2024). Rainfall Observation Leveraging Raindrop Sounds Acquired Using Waterproof Enclosure: Exploring Optimal Length of Sounds for Frequency Analysis. Sensors, 24(13), 4281. https://doi.org/10.3390/s24134281

Joly, D., Brossard, T., Cardot, H., Cavailhes, J., Hilal, M., & Wavresky, P. (2010). Les types de climats en France, une construction spatiale. Cybergeo. https://doi.org/10.4000/cybergeo.23155

Kouadio, K. Y., Aman, A., Ochou, A. D., Ali, K. E., & Assamoi, P. A. (s. d.). Rainfall Variability Patterns in West Africa: Case of Cote d'Ivoire and Ghana.

Metcalf, O. C., Lees, A. C., Barlow, J., Marsden, S. J., & Devenish, C. (2020). hardRain: An R package for quick, automated rainfall detection in ecoacoustic datasets using a threshold-based approach. Ecological Indicators, 109, 105793. https://doi.org/10.1016/j.ecolind.2019.105793

https://doi.org/10.5194/egusphere-2026-3457
Preprint. Discussion started: 18 August 2026

Peleg, N., Torelló-Sentelles, H., Mariéthoz, G., Benoit, L., Leitão, J. P., & Marra, F. (2023). Brief communication: The potential use of low-cost acoustic sensors to detect rainfall for short-term urban flood warnings. Natural Hazards and Earth System Sciences, 23(3), 1233–1240. https://doi.org/10.5194/nhess-23-1233-2023

Pinho, P. F., Silvestrini, R., Fellows, M., Perez, L., Alencar, A., Guyot, C., Moutinho, P., Lapola, D., & Stringer, L. (2025). “Vulnerabilities and compound risks of escalating climate disasters in the Brazilian Amazon”. Nature Communications. https://doi.org/10.1038/s41467-025-66603-0

Rácz, T., & Waltner, I. (2023). A Review and Categorization of Rain Depth and Rainfall Intensity Measurement Methods. Tájökológiai Lapok, 21(2), 116–135. https://doi.org/10.56617/tl.4958

Reboita, M. S., Gan, M. A., Rocha, R. P. D., & Ambrizzi, T. (2010). Regimes de precipitação na América do Sul: Uma revisão bibliográfica. Revista Brasileira de Meteorologia, 25(2), 185–204. https://doi.org/10.1590/S0102-77862010000200004

Schleiss, M., & Berne, A. (2010). Identification of Dry and Rainy Periods Using Telecommunication Microwave Links. IEEE Geoscience and Remote Sensing Letters, 7(3), 611–615. https://doi.org/10.1109/LGRS.2010.2043052

Virtanen, P., Gommers, R., Oliphant, T. E., Haberland, M., Reddy, T., Cournapeau, D., Burovski, E., Peterson, P., Weckesser, W., Bright, J., Van Der Walt, S. J., Brett, M., Wilson, J., Millman, K. J., Mayorov, N., Nelson, A. R. J., Jones, E., Kern, R., Larson, E., … Vázquez-Baeza, Y. (2020). SciPy 1.0: Fundamental algorithms for scientific computing in Python. Nature Methods, 17(3), 261–272. https://doi.org/10.1038/s41592-019-0686-2

Wang, M., Chen, M., Wang, Z., Guo, Y., Wu, Y., Zhao, W., & Liu, X. (2024). Estimating rainfall intensity based on surveillance audio and deep-learning. Environmental Science and Ecotechnology, 22, 100450. https://doi.org/10.1016/j.ese.2024.100450

Wang, X., Glade, T., Schmaltz, E., & Liu, X. (2023). Surveillance audio-based rainfall observation: An enhanced strategy for extreme rainfall observation. Applied Acoustics, 211, 109581. https://doi.org/10.1016/j.apacoust.2023.109581

Wang, X., Zhao, K., Zhou, A., Huang, H., & Chen, H. (2026). “Hearing” Wind Speed: Ground Wind Measurement Using Deep Learning From Surveillance Audio. Geophysical Research Letters, 53(3), e2025GL119370. https://doi.org/10.1029/2025GL119370

Wang, Y., Jiang, H., Liu, G., Chen, Q., & Ni, M. (2026). Research on Real-Time Rainfall Intensity Monitoring Methods Based on Deep Learning and Audio Signals in the Semi-Arid Region of Northwest China. Atmosphere, 17(2), 131. https://doi.org/10.3390/atmos17020131

World Meteorological Organization. (2025). Early Warnings for All in Focus: Hazard Monitoring and Forecasting. United Nations.

Xavier, R. S., Gosset, M., Maciel, T. F., Bicudo, T., Nascimento, L. A. D., Ramalho, E., & Fleischmann, A. (2024). Measuring Amazon Rainfall Intensity With Sound Recorders. Geophysical Research Letters, 51(20), e2024GL108210. https://doi.org/10.1029/2024GL108210